Nanoarchitectonics
http://ojs.wiserpub.com/index.php/NAT/

UNIVERSAL WISER PUBLISHER

Research Article

A Free Space Characterisation of CNT-Epoxy Based Nanocomposites Using Patch Antennas

Sebastian Tamayo-Vegas[1*], Khalid Lafdi[1,2], Michael Elsdon[3]

[1]Department of Mechanical Engineering, Northumbria University, Newcastle upon Tyne NE1 8ST, UK
[2]Department of Chemical Engineering, University of Dayton, Dayton, OH 45469, USA
[3]Smart Materials and Surfaces Laboratory, Northumbria University, Newcastle upon Tyne NE1 8ST, UK
E-mail: w18002002@northumbria.ac.uk

Received: 2 September 2022; **Revised:** 7 February 2023; **Accepted:** 10 April 2023

Abstract: The influence of nanofillers percentage on a patch antenna return loss (RL) was investigated through experimental and numerical analysis. Free space measurements were carried out on six samples reinforced with carbon nanotubes (CNTs) containing 0, 0.5, 1, 2, 4 and 5 wt%. The experimental measurements were obtained using a vector network analyser (VNA) and a patch antenna with a resonance frequency of 5 GHz and a fractional bandwidth of 3%. The antenna field regions were calculated and the samples were tested at the reactive, radiating near-field, and far-field. The findings indicate distinctive behaviours. At the reactive near-field region, the CNTs, as expected, seem to diminish the RL values around resonance frequencies. On the contrary, at radiating near-field and far-field, the CNTs provoke the variation of RL in the antenna bandwidth according to their percentage. Especially after the electrical percolation threshold (EPT). Moreover, a numerical study was performed. Using the finite element method (FEM) and an idealized model of the RL behaviour values were simulated. At higher CNTs percentages (i.e., EPT), unique behaviours were found. The alteration in the key electromagnetic properties is confirmed in experimental and numerical studies.

***Keywords*:** CNTs, computational modelling, free space measurements, reflectivity, RL

1. Introduction

Since the discovery of carbon nanotubes (CNTs) in 1991 [1], great enthusiasm prevails within the research community [2]. As technologies advance, the CNTs usage in numerous industries keeps arising every year. It is forecasted that these nanofillers will continuously allow the development of cutting-edge technologies such as emission displays, artificial muscles, energy storage, nano-sized multifunctional sensors, and artificial muscles [3-5]. Specifically, they are used as an empowering material for polymeric nanocomposites (PMNC). CNTs are employed to enhance pristine materials as they pose outstanding properties, i.e., mechanical, electrical, and thermal [6, 7]. These properties are ideal to reinforce polymeric matrices whose properties are often mediocre. CNTs properties are beneficial and not limited to aerospace, medicine, aeronautics, and military applications [8, 9]. The desired final properties rely on the aspect ratio, filler aggregation and interphase properties [6, 10-16].

In electronics, for instance, they are used to produce new conductive and semiconductive materials, which are treasured in diverse fields. The excellent electrical properties of the CNT benefit the insulator material. This effect is due to small percentage of CNTs alter the composite permeability, and permittivity, among others. The electromagnetic

DOI: https://doi.org/10.37256/nat.4220233463

properties are essential for many applications in, active sensors, antenna design, electromagnetic interference (EMI) shielding, lightning-strike, radio frequency identification (RFID) and electromagnetic absorption.

There are various methods for measuring the electromagnetic properties of materials. These methods normally use a vector network analyser (VNA). They are classified as transmission/reflection line method, opened-ended coaxial probe method, free space method and resonant method. These are capable to characterise the electromagnetic material's properties at various frequencies. Each approach shows intrinsic advantages and disadvantages. Free space methods, for example, are extremely attractive as they offer a non-destructive and contactless approach. Allowing characterisation in their work environment. Advantageous for materials exposed to harsh environments, i.e., high temperatures, salinity atmospheres, and acid attacks [9, 17-19].

Free space methods can also be performed in a wide range of frequencies as it employs the usage of an antenna to characterize the material. This is an advantage for example the electric permittivity and permeability are frequency dependent [20, 21]. Moreover, as the antenna theory dictates, there are different regions on the antennas and thus potentially different influences. Distinguishing the characterisation between these regions is important for the above-mentioned applications and especially in electromagnetic compatibility (EMC) applications and RFID tags, and active chip-less sensors. Some exclusively work in the reactive near-field region [22-24]. Thus, characterising materials in different regions is beneficial for a wide range of applications. Also, with the facility of antenna design several frequencies can be explored. In the same manner, there is a huge decrement on the price of the antenna compared with it counterpart waveguides, usually expensive.

In this study, we have measured the scattering parameters of PMNC with different percentages of CNTs. Six different samples containing different percentages of CNT were analysed with the free space measurement method. The analysis was performed utilizing a patch antenna with a resonance frequency of 5 GHz and a fractional bandwidth of 3%. A VNA was used to determine the behaviour in the frequency range of 3 GHz to 6 GHz. The samples were placed within the antenna field regions to explore different effects. Moreover, a numerical analysis was performed using finite element method (FEM) to solve the Maxwell equation with the frequency domain solver using CST Studio software. The results were presented independently for each region. The studies suggest that the behaviour of the antenna at the bandwidth regions are changed and noticeable at every percentage. The well-known key electromagnetic parameters are the electrical conductivity and the dielectric constant of the specimens that are affected by the weight percentage [10, 11, 21, 25]. This research focused on the effects that the percentage of CNTs can have in the final materials properties, which often the expected multifunctional properties lack any improvement. The employment of a patch antenna is effective to confirm the electromagnetic difference among the samples

2. Materials and methods

2.1 *Basic principles of free space and antenna field regions*

Free space measurement is described as a technique which allows measurements of the electromagnetic properties through scattering parameters at a wide range of frequencies. This technique involves the usage of VNAs from which a signal at a single frequency is swept to the material under test (MUT) and tuned to detect the response signals arising from the material [26-30].

In the VNA, the return loss (RL) and transmission loss (TL) are respectively calculated at the desired frequencies [26]. In this work, the RL was calculated at the antenna field regions, e.g., reactive near-field, radiating near-field and far-field (Figure 1) [31, 32].

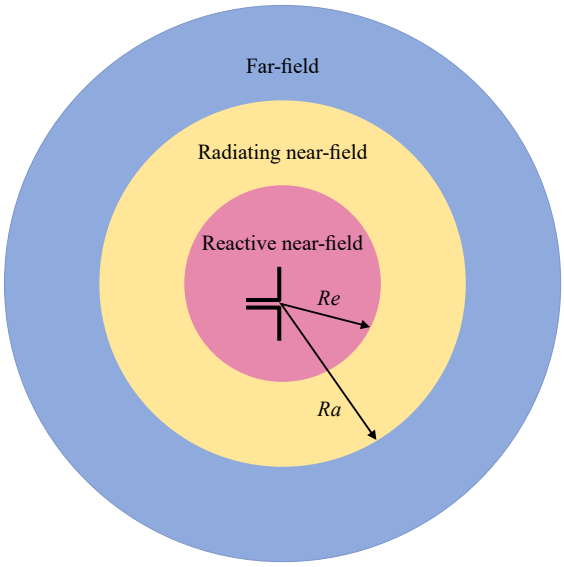

Figure 1. Antenna field regions

Although in these surrounding spaces, there are no abrupt changes in the antenna field configurations, there are distinct behaviours [31]. These unique boundaries were calculated with Equations (1) and (2) defined by near and far-field antenna theory [33-35]. Where D is the largest dimension of the antenna and λ is the wavelength. The obtained distance was 6.3 mm for reactive near-field, 11 mm for radiating near-field, and far-field any distance bigger than Ra. Accordingly, the specimens were placed within these regions changing $D1$ value (Figure 2).

$$Re = 0.62\sqrt{\frac{D^3}{\lambda}} \tag{1}$$

$$Ra = 2\frac{D^2}{\lambda} \tag{2}$$

2.2 *Materials and samples preparation*

In this study, six specimens containing CNTs fractions of 0%, 0.5%, 1%, 2%, 4% and 5% by weight were considered for free space characterisation. The sample matrix was made of a commercial Epoxy EPON 862. The CNTs consist of multi-wall carbon nanotubes (MWCNTs) purchased from Applied sciences Inc. The MWCNTs diameter and length range from 30 µm to 100 µm and 20 nm to 100 nm respectively. The sample fabrication consists of shear mixing the CNTs in an ultrasonic bath in acetone for a period of 1 hour. Thereafter, the epoxy resin was steadily added while continuously mixing until the solvent was evaporated. Finally, the mixture was poured into a silicone mould and hot-pressed in a vacuum. The sample's dimensions were 80 mm in width, 52 mm in length, and 6 mm thick.

2.3 *Experimental procedure*

The electromagnetic characterisation was performed using a Network Analyzer Agilent N230A at room temperature (25 °C). Two 85131F flexible cables were connected to port 1 and port 2. The calibration was performed using the ECal Agilent N3360 Calibration Kit. The free space measurements were performed using a patch antenna with a resonance frequency of 5 GHz. The measurements were performed in the frequency range from 3 GHz to 6 GHz. First, the RL of the antenna was obtained in free space. Thereafter, the RL parameter was obtained, whilst placing the sample at each field region three times per specimen. The experimental setup is shown in Figure 2.

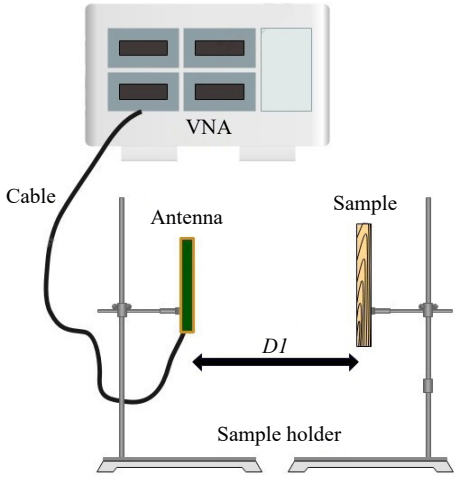

Figure 2. Experimental setup

2.4 *Numerical procedure*

The numerical simulations were performed using CST Studio software. An idealized model was built. The finite element analysis (FEA) was performed in the frequency domain solver using CST Studio [36]. The simulations also involved the three field antenna regions. The samples were placed in front of the antenna with the calculated distances (shown in Figure 3). At each region, the approach was setting the electrical conductivity of each sample according to Table 1 [11]. Subsequently, the dielectric permittivity of the samples was set to follow a sweep from 2 to 6 at a step of 0.11 unit for a total of 720 simulation runs. Each influence curve was recorded and compared with experimental results. Finally, the best fit of the data is separately compared with the experimental at each region and each sample.

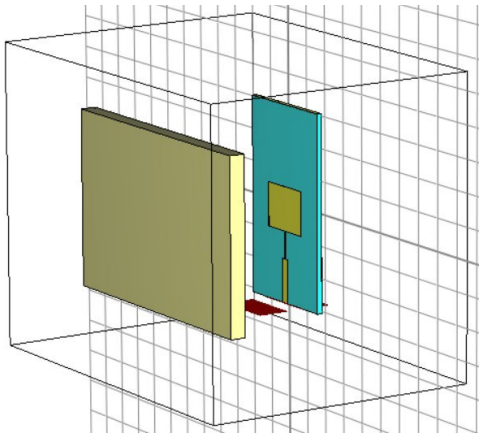

Figure 3. Numerical simulations setup

3. Results and discussion

In this section, the experimental and numerical results are presented. The section is divided into three different antenna field regions. At each region, the experimental results are presented and posteriorly divided into two approaches: before and after electrical percolation threshold (EPT). At each section, the electrical conductivity of the samples and the percolation percentage (i.e., 2 wt%) were pre-set according to our previous study and are presented in Table 1 [11]. Also, we discussed the potential alteration of the dielectric constant in each sample. Additionally, the experimental

results, along with the modelling, were also discussed within these considerations. These sections were organized to facilitate the narrative of CNTs properties, (e.g. aggregates, agglomerates, orientation) and their influence on the antenna RL at the field regions.

Table 1. Samples of electrical conductivity (S/cm) values

Samples CNT (wt%)	Electrical conductivity (S/cm)
0	2.123×10^{-7}
0.5	2.123×10^{-5}
1	5.195×10^{-4}
2	0.2512
4	3.472
5	5.549

3.1 *Reactive near-field*

In Figure 4, the experimental results are presented. The antenna RL is shown. This measurement was acquired by placing the antenna with no interference. The curve profile is then compared to the six samples placed at the reactive near-field region. Figure 4(b) and 4(c) represent the samples before and after the percolation threshold. As expected, the experimental data shows a clear alteration in the antenna RL within the bandwidth region. According to antenna theory, in this region, the electric and magnetic fields are not yet perpendicular to each other. However, the electric and magnetic material properties alter the forming fields. When placed in these regions, the antenna Q factor seems to reduce. The addition of CNTs to the epoxy matrix, altering its electromagnetic properties seems to be intense enough to act in the antenna fields, revealing changes an annulling RL values. The CNT's weight percentage influences the RL accordingly.

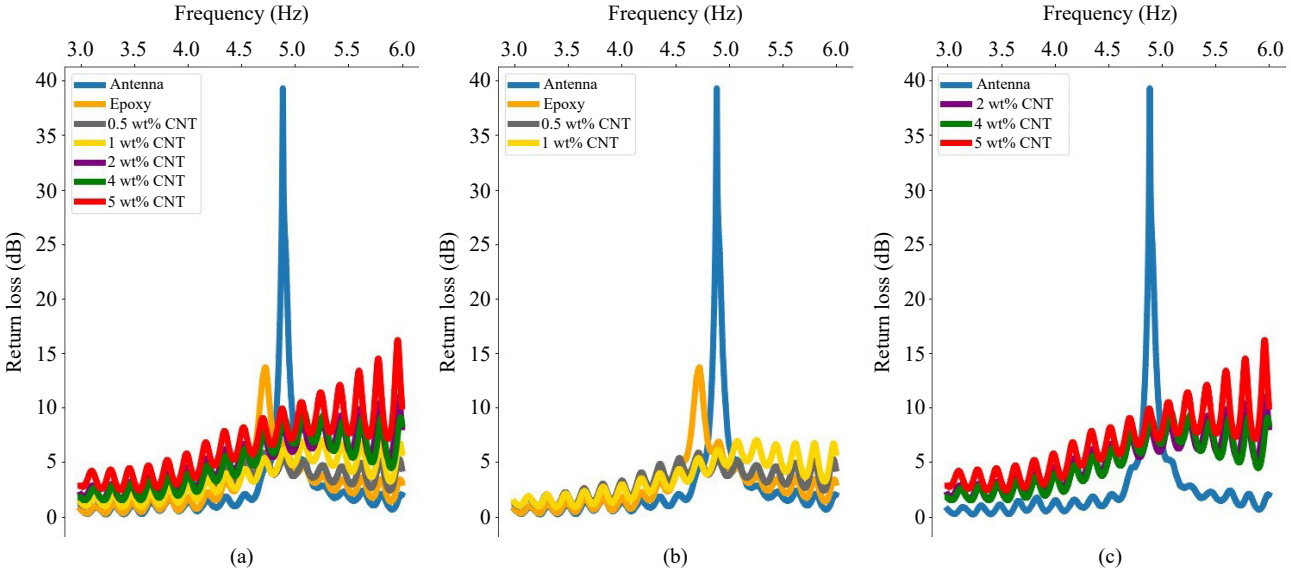

Figure 4. Reactive near-field experimental results: (a) all samples; (b) before percolation threshold; (c) after percolation threshold

The numerical behaviour at the reactive field is presented in Figures 5 and 6 respectively. Following the same approach, the results have been divided into before and after percolation thresholds. Also, each sample result is

presented for every numerical constant sweep. In this region, the same behaviour appears. Also, the experimental data shows small RL values, only reaching higher and distinctive behaviour after the EPT. The numerical result before EPT is shown in Figure 5. The pristine epoxy experimental data reaches 14 dB at its central resonance, whereas the numerical is close to 8 dB. The experimental data shows peaks through its curve due to the accuracy of the VNA. However, the numerical curve appears to follow a very close path to the experimental data.

Figure 5(c) and 5(d) depict the behaviour of the samples containing 0.5 wt%. At this low percentage, there is experimental and numerical agreement. The variation of the RL reaches 6 dB. This is also seen in Figure 5(e), where the dielectric constant is shown for the sample containing 1 wt%. The experimental data reached a low value of 7 dB. Whereas the numerical just pass the 6 dB benchmark. Although, there is a disagreement in the final values the model predicts the augmentation of RL values from 6 dB to 7 dB. The samples after the percolation threshold are shown in Figure 6. The highest values shown in the experimental data are just achieved at 6 GHz. However, if there is a comparison in the bandwidth region the obtained values are quite similar. For instance, the model shown in Figure 6(a) represents the sample containing 2 wt% of CNTs. In Figure 6(b), the best fit is shown. It is clear that in the first part of the profile curve, the model is capable to predict the behaviour. Additionally, the lowest value found in resonance frequency experimental and numerically is around 7 dB. A better performance of the model is found with the sample containing 4 wt%. The profile seems to follow a closed path. Besides the highest values are closely predicted with the different constants. The alteration found in samples 4 and 5 wt% is close in values. The latter is shown in Figure 6(e) and 6(f). Although the model is still close to the value of 8 dB, the dielectric constant plays a big role as the electrical conductivity reaches the EPT. The experimental value is shown as a 10 dB maximum decrement. Where in the modelling approaching 8 dB. At this region, the modelling is not capable to predict the minimum changes that are shown in the experimental data. It seems that the in the reactive field the FEM lacks the potential influence of the intrinsic characteristics of CNTs. The lack of formation of the electrical and magnetic field seems to affect the models' predictions.

3.2 *Radiating near-field*

In Figure 7, experimental results of radiating near-field are presented. Figure 7(a) depicts the sample's influence on the patch antenna signal. The frequency ranges are from 3 GHz to 6 GHz. It is clear that as the percentage of CNT the RL decreases in a steady and ascendant path. Subsequently, in Figure 7(b) and 7(c), the results are breakdown into two parts, corresponding to the EPT percentage. In Figure 7(b), the specimens of pristine epoxy, 0.5 wt%, and 1 wt% are presented as they remain in the area below the EPT. The experimental results show that the pristine specimen starts to alter the maximum RL value of the antenna, first, it switches the RL curve to the right and reduces the RL value. This phenomenon is also seen as the CNTs percentage is augmented. The RL value of the antenna (39 dB) is reduced with each sample. Below the EPT, the specimens seem to alter the RL curve similarly. The area of influence of the three samples remains around the same values. Altering the RL values to 27 dB, and 25 dB for the samples containing 0.5 wt% and 2 wt% respectively. In Figure 7(c), the samples after EPT are presented. A clear alteration phenomenon is present after EPT. Nevertheless, it presents an even increment in the Q factor on the RL curve. The samples of 2 wt%, 4 wt% and 5 wt% orderly affect the decrement on the RL of the antenna. The sample of the 2 wt% presents a RL value of 24 dB. This value goes down to 20 dB for 4 wt% and 18 dB for the sample containing 5 wt%.

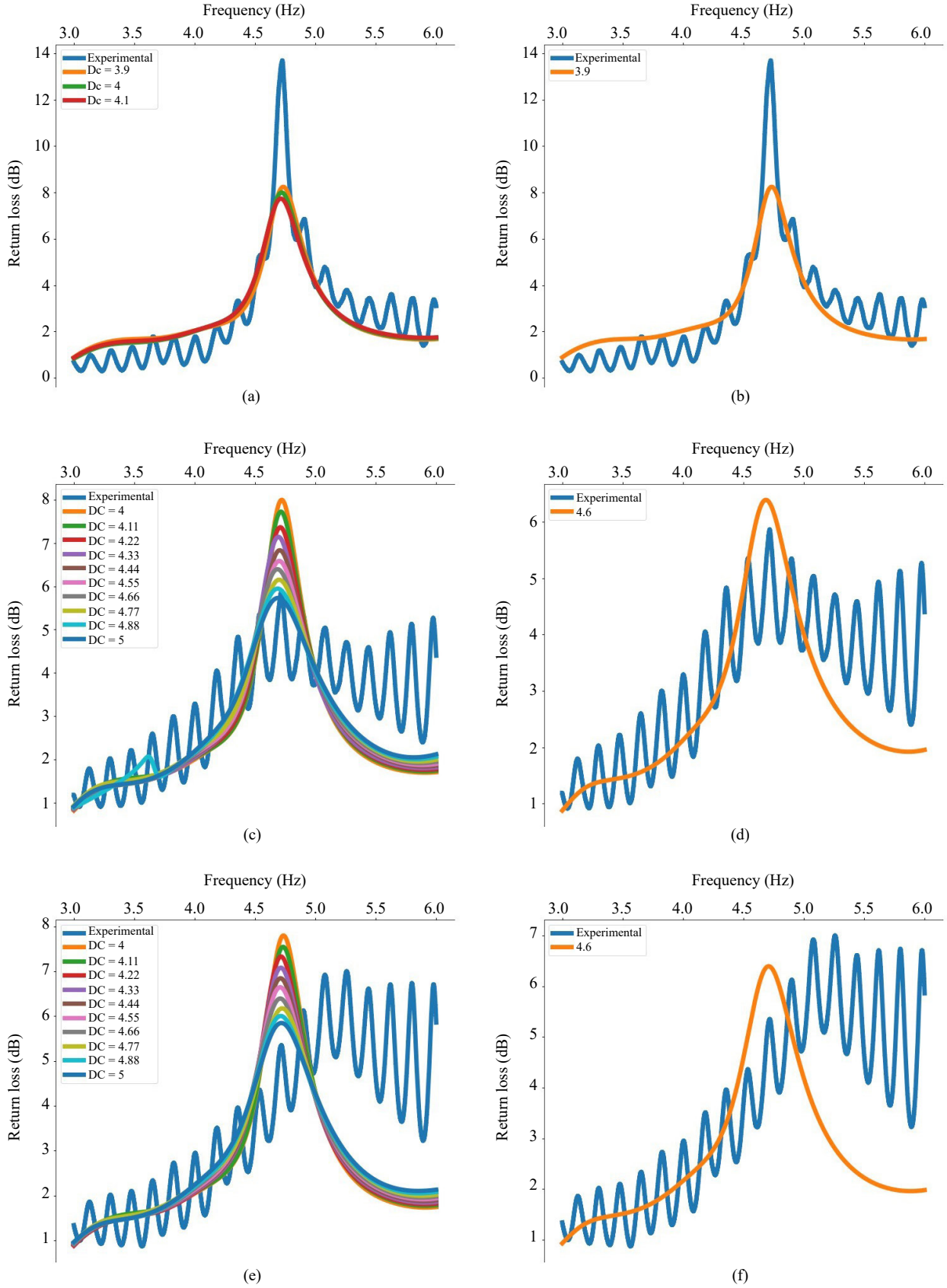

Figure 5. Reactive near-field numerical vs. experimental results: (a) epoxy; (b) epoxy best fit; (c) 0.5 wt%; (d) 0.5 wt% best fit; (e) 1 wt%; (f) 1 wt% best fit

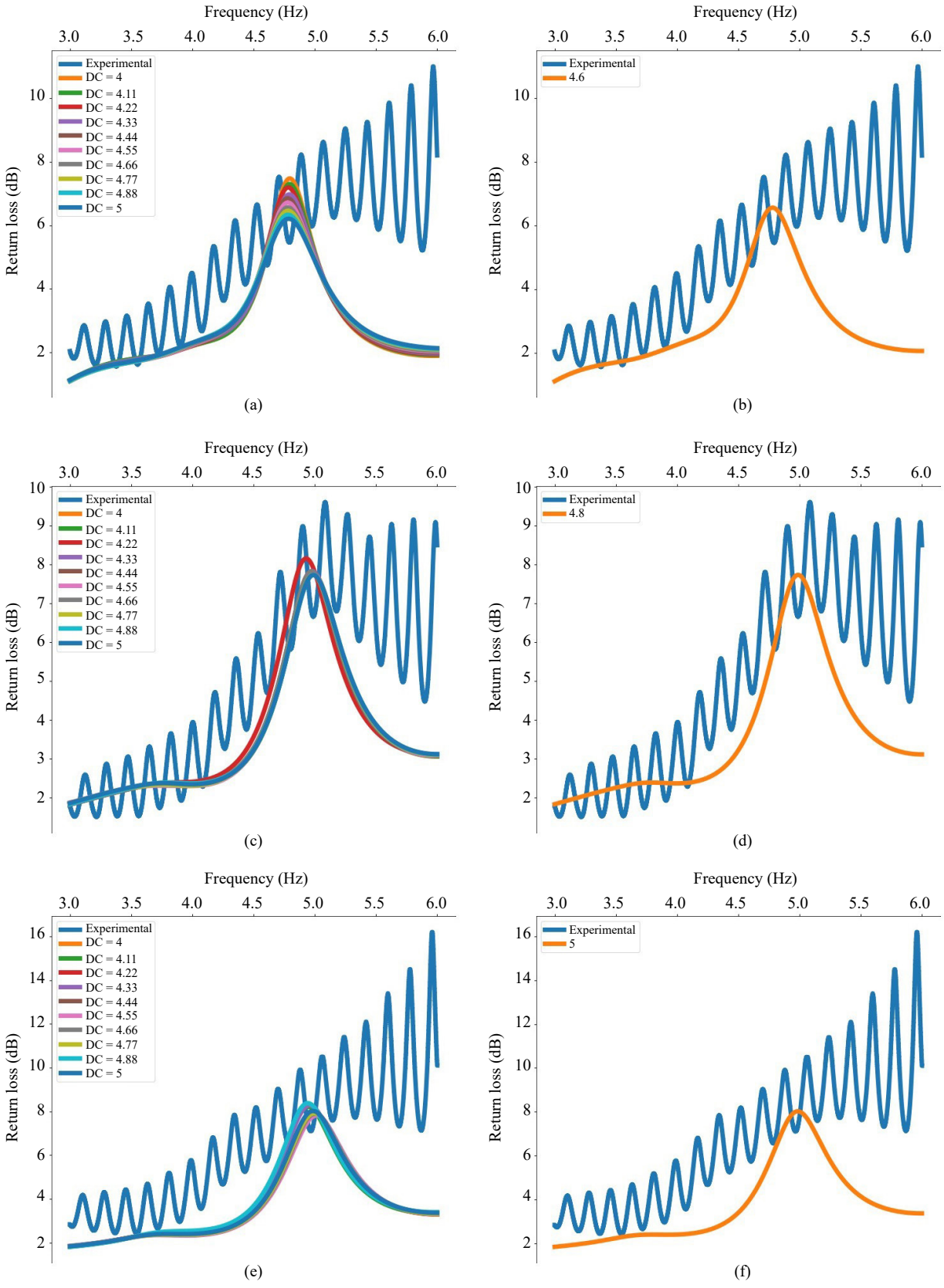

Figure 6. Reactive near-field numerical vs. experimental results: (a) 2 wt%; (b) 2 wt% best fit; (c) 4 wt%; (d) 4 wt% best fit; (e) 5 wt%; (f) 5 wt% best fit

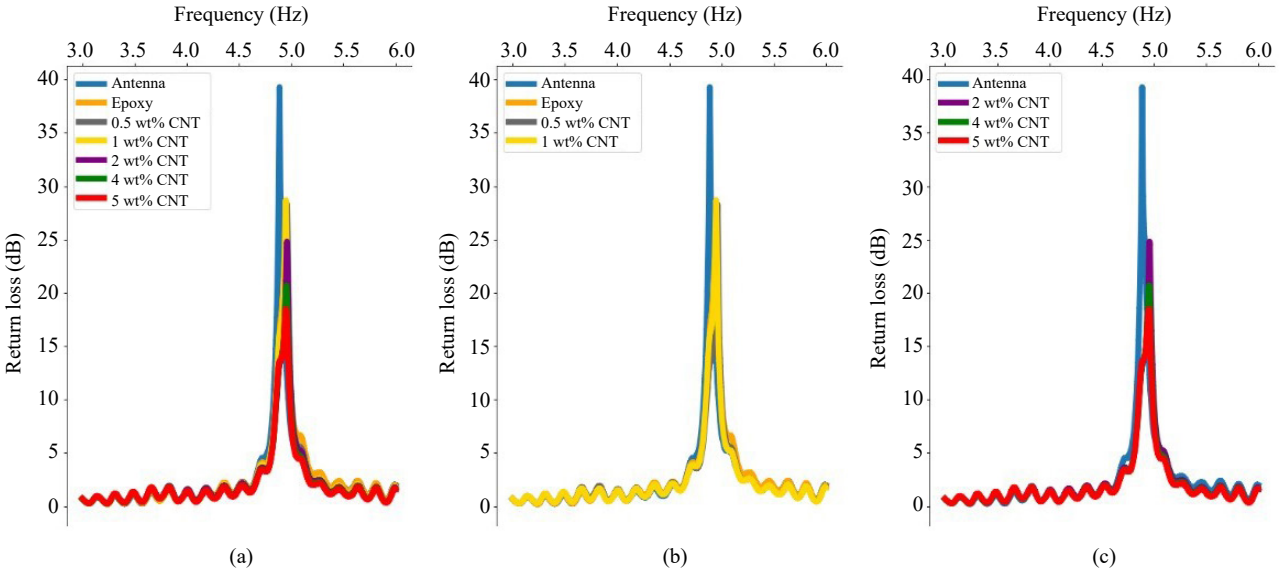

Figure 7. Radiating near-field experimental results: (a) all samples; (b) before percolation threshold; (c) after percolation threshold

The numerical modelling is shown in Figures 8 and 9. Figure 8 shows the numerical results before EPT. Figure 8(a) shows the pristine epoxy along with three potential dielectric constant numbers. According to the manufacturing data, the dielectric constant oscillates between 3.9 to 4. Thus, three sweep simulations were performed with 3.9, 4 and 4.1. Figure 8(b) shows the best fit of dielectric constant 3.9 following numerical and experimental data. Figure 8(c) and 8(d) show the numerical results for the first sample containing CNTs. The addition of 0.5% seems to alter the dielectric constant of the sample. The experimental results showed a RL value reduction to 27 dB. In the numerical results, the values range from 22 dB to 27 dB. Although the match is obtained at 27 dB, the perfect fit is with a dielectric constant of 4.6 shown in Figure 8. At this addition point, the model seems to overestimate the addition of CNTs, even matching the results of 1% addition. At this lower percentage, the numerical predictions follow the same phenomenon seen in the experiment. The area of influence of the small addition remains in the same range of RL values. The last specimen before EPT is shown in Figure 8(e) and 8(f). The range RL value for different dielectric constants oscillates from 22.8 dB to 27.5 dB, slightly changing the values of the previous specimen. However, following the alteration path in an orderly manner.

Figure 9 presents the results after EPT (i.e., 2 wt%, 4 wt%, and 5 wt%). The results are presented in two parts. Firstly, the experimental results vs. the numerical modelling following the parameter sweep for the dielectric constant from 4 to 5. In the second part, the best fit for each sample is presented in Figure 9(b), 9(d), and 9(e). Figure 9(a) and 9(b) depict the experimental and numerical results of the 2 wt% sample. After EPT, the sample containing 4 wt% is the first sample that seems to acquire a higher value of dielectric constant following the same EPT phenomenon. The changes sweep changes seem to closely follow the RL experimental curve. The changes on the dielectric seem to alter the final RL value.

Although there is a divergence in the final data between experimental and numerical, the model is capable to predict the reduction of the antenna RL 35 dB. The data show a RL reduction range from 26 dB to 30 dB constant. The experimental data showed a reduction to 24 dB, which in simulation the closes will be with the dielectric constant of 4 similar to the samples before EPT, however, the best curve fit is the modelling with the dielectric constant of 4.66, showing a slight augmentation on the final dielectric constant.

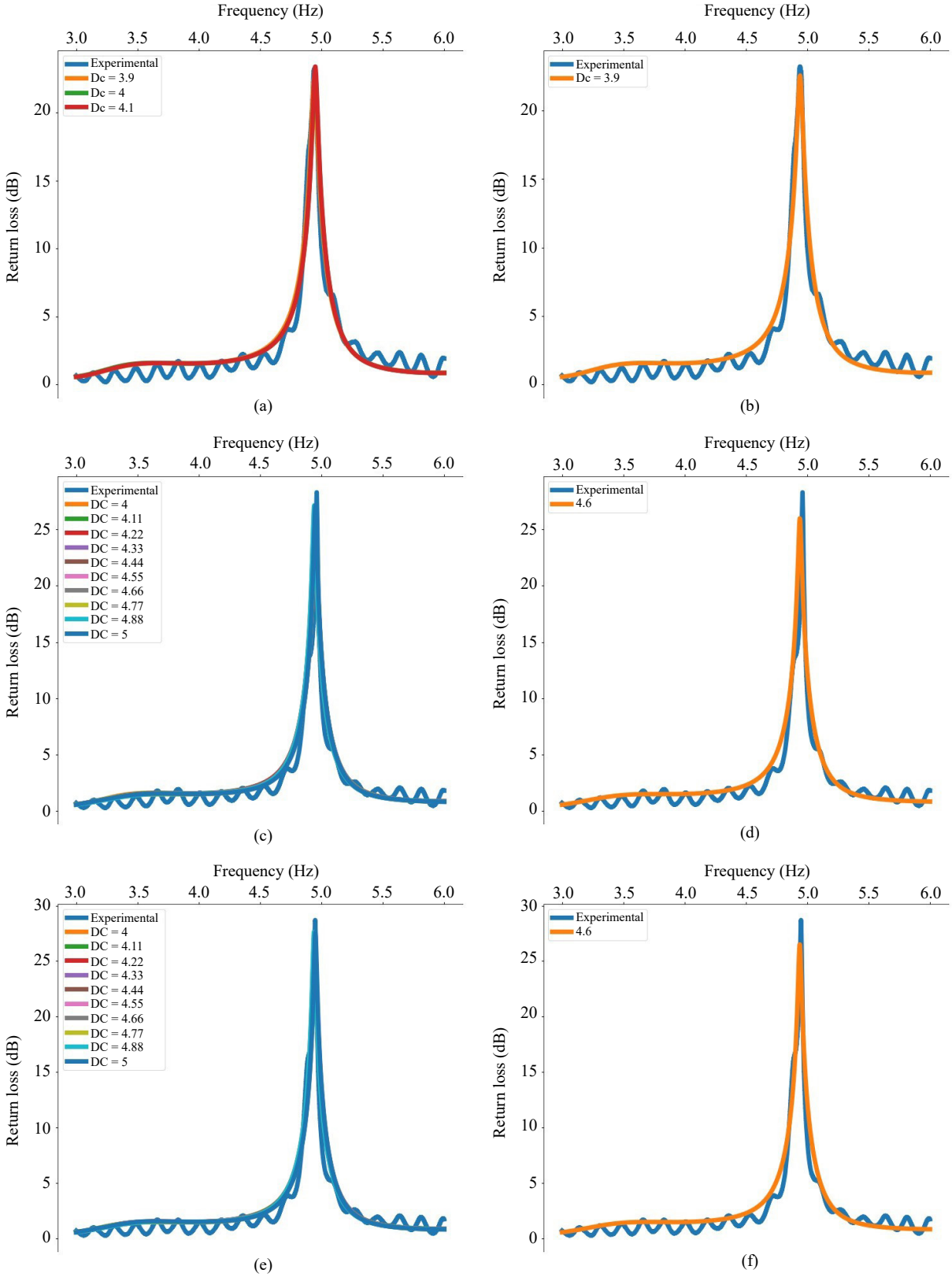

Figure 8. Radiating near-field numerical vs. experimental results: (a) epoxy; (b) epoxy best fit; (c) 0.5 wt%; (d) 0.5 wt% best fit; (e) 1 wt%; (f) 1 wt% best fit

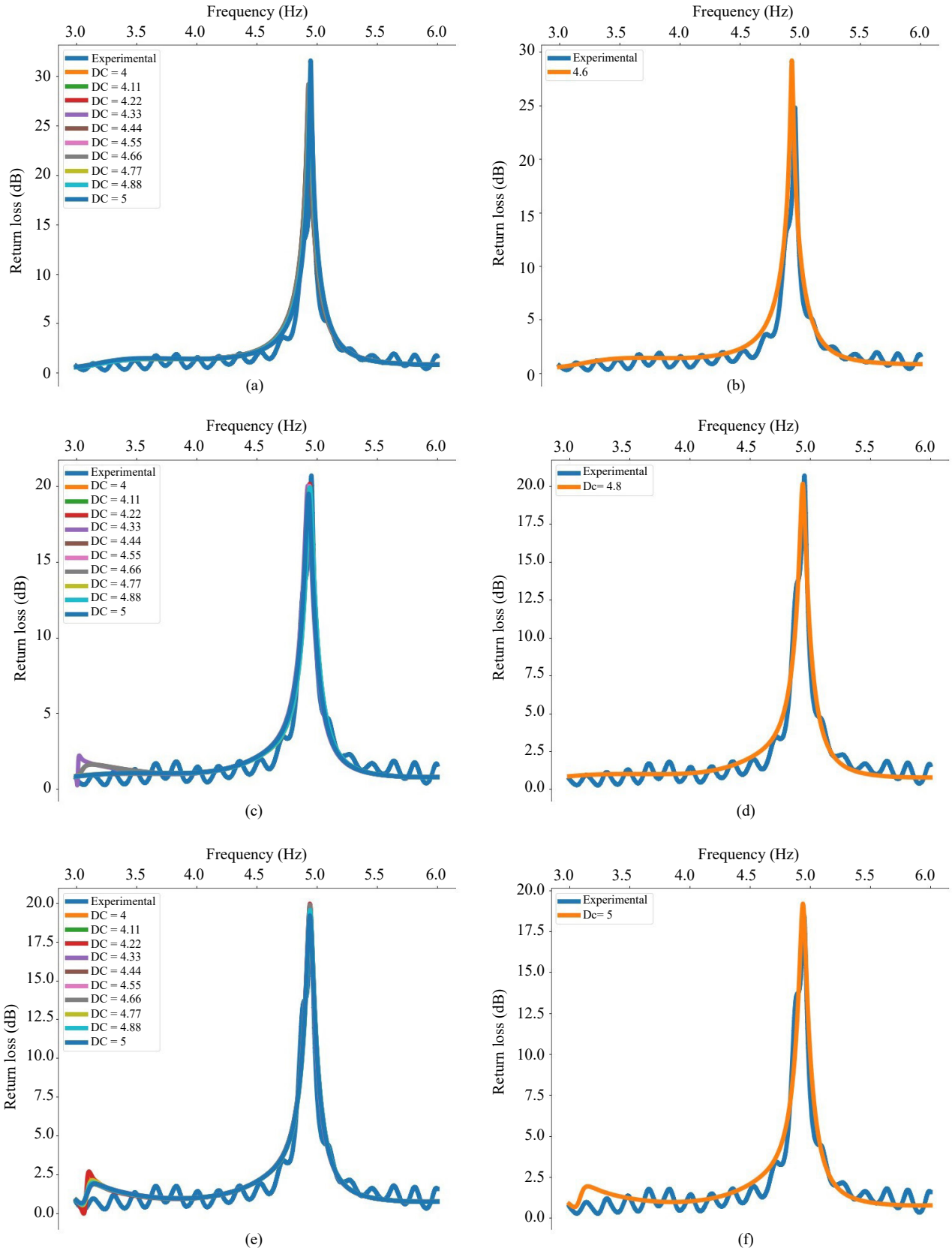

Figure 9. Radiating near-field numerical vs. experimental results: (a) 2 wt%; (b) 2 wt% best fit; (c) 4 wt%; (d) 4 wt% best fit; (e) 5 wt%; (f) 5 wt% best fit

Following the same approach, Figure 9(c) and 9(d) shows the results for the 4 wt% sample. In this case, the modelling shows a better prediction of the properties. The RL reduction range from 19 dB to 20 dB. For this case, we can see that the CNTs also alter the direction of the resonance frequency from 4.92 GHz to 4.94 GHz. Thus, to predict the experimental behaviour in Figure 9(c), the best fit is with a dielectric constant of 4.88. Regarding the RL, the experimental value showed 20 dB which is predicted with the numerical simulations. Ultimately, the sample with 5 wt% of CNTs is shown in Figure 9(e) and 9(f). A similar phenomenon is seen. The addition of the CNTs also alters the resonance frequency, however, the best fit was found to be with a dielectric constant of 5, following an expected decremental trend. Regarding the RL values the reduction oscillates from 19 dB to 19.9 dB whereas the experimental showed 18 dB.

3.3 *Far-field*

Figure 10 represents the experimental data for the far antenna field region. In this region, the CNTs influence alters the antenna RL similarly to that near radiating field. However, as it can be seen the RL curve in this case seems to be reduced the RL, altering the antenna resonance frequency to around 4.8 GHz. Similarly, the RL value decreases as the CNT content increases. The results are presented in Figure 10(a) for the six samples. Figure 10(b) and 10(c) show the behaviour before and after the percolation threshold respectively. In this case, before EPT of the epoxy, 0.5 wt% and 1 wt% provoke almost the same behaviour in the RL value. The antenna RL of 39 dB goes down to 24.9 dB for the sample containing 0.5 wt% and to 24.78 dB for samples containing 1 wt%. At this low CNT percentage, there is a clear reduction of the antenna RL, however, the RL values change slightly. Conversely, the values after EPT change in a more distinctive manner. Figure 10(c) shows the samples 2 wt%, 4 wt% and 5 wt%. It is clear that as the percentage goes up the RL curve goes up in an descendant-expected path. The violet curve shows the 2 wt% specimens showing a RL value of 23 dB. This values down up to 22 dB for the 4 wt% percentage. Finally, the value reaches 21 dB for the specimen containing 5 wt%.

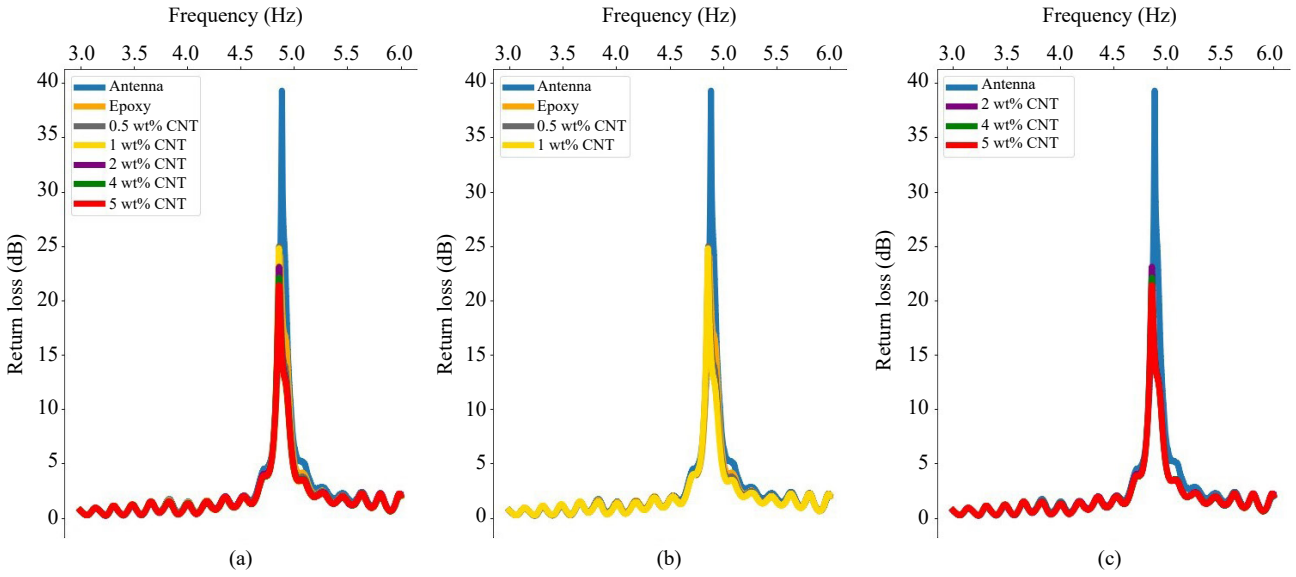

Figure 10. Far-field experimental results: (a) all samples; (b) before percolation threshold; (c) after percolation threshold

The numerical far-field results before EPT are presented in Figure 11. The numerical results are compared with the experimental data. As can be seen, the model in this region overestimates the influence on the RL values. For instance, for the pristine epoxy sample, the dielectric constant of 3.9 seems to be close to the experimental. Yet, it alters the RL value up to 21 dB, whereas the experimental was found to be 25 dB. Following these criteria the numerical model for the sample of 0.5 wt% is presented in Figure 7(c) and 7(d). The changes in the dielectric constant seem to overestimate

the influence on the antenna attenuation.

The attenuation values range from 21 dB to 18 dB. The best fit was found to be 4.6 which showed a value of 18.5 dB. Comparing to the experimental (24 dB) there is a mismatch of six points. This phenomenon seems consistent for the last sample. The sample containing 1 wt% produces a similar effect in the modelling and the experimental. The obtained value was 18.6 dB, barely any different from the previous sample. This is also presented in the experimental data, where before the percolation threshold the samples seem to produce similar disturbance in the RL. However, there is a potential order found in the numerical data from 18.5 dB and 18.6 dB and the experimental from 24.78 dB to 24.9 dB. Showing that at a low CNT percentage, the sample dielectric constant remains the same at around 4.6.

Figure 12 shows the far-field region of samples after the percolation threshold. The effects of the electrical conductivity and dielectric constant seem to produce a great reduction within the numerical modelling using CST Studio software. The sample of 2 wt% is shown in Figure 12(a) and 12(b). The latter shows the best fit after the dielectric constant sweep. Following the previous antenna regions, the samples seem to accommodate the values of dielectric constant ranging from 4 to 5. For instance, the dielectric constant of 4.6 disturbs the antenna RL value to 18 dB for 2 wt% and to 15 dB for 4 wt% samples. The latter seems to follow the orderly trend found in the experimental data from 23 dB, 22 dB and 21 dB for 2 wt%, 4 wt% and 5 wt% respectively. Finally, the sample containing the most CNTs (i.e., 5 wt%) is shown in Figure 12(e) and 12(f). At this high percentage, the experimental value reached 21 dB whereas the simulated value was 14 dB. Nevertheless, the model still predicts the orderly decrease of the antenna RL value from 18 dB, 15 dB and 14 dB for 2 wt%, 4 wt% and 5 wt% respectively.

4. Conclusion

The RL of PMNC reinforced with MWCNT was investigated using experimental and numerical approaches. Employing the free space method six samples containing different percentages of CNTs were characterised using a patch antenna and a VNA. The RL was recorded at the three antenna regions. Using FEA, the analysis was performed and compared with the experimental data. The data suggest that there is a distinctive behaviour from the reactive to the radiating near-field and far-field. The former seems to be altered in a manner that the RL diminishes as the CNTs percentage increases. Because of the intrinsic properties of the CNTs which alters the electric and magnetic fields. On the other hand, in the radiating nearfield and far-field a more expected behaviour was found. As the percentage of CNTs augments the RL decreases accordingly. This is due to an increase in the CNT filler content which increases the electrical conductivity and the sample intrinsic wave impedance decreases [26]. In the computational model, the electrical conductivity and the dielectric constant were the factors that influence the RL behaviour the most. At the reactive region, the model fails to predict the behaviour of the experimental sample. However, a good understanding of the dielectric constant of the sample was obtained. Experimentally, far-field region showed a sharper distinction to characterise the samples with different percentages of CNTs. However, numerically the modelling overestimates the influence of the electrical conductivity and dielectric constant. The influence seems to follow the same order path, however, a mismatch in the RL values was seen. The radiating near-field seems to be the perfect area where a perfect distinction with the different percentages of CNTs was seen. Also, better accuracy in the numerical data was found in this region. Finally, the study suggested that a free space method is suitable for the characterisation of composite materials where non-destructive and contactless approaches are needed.

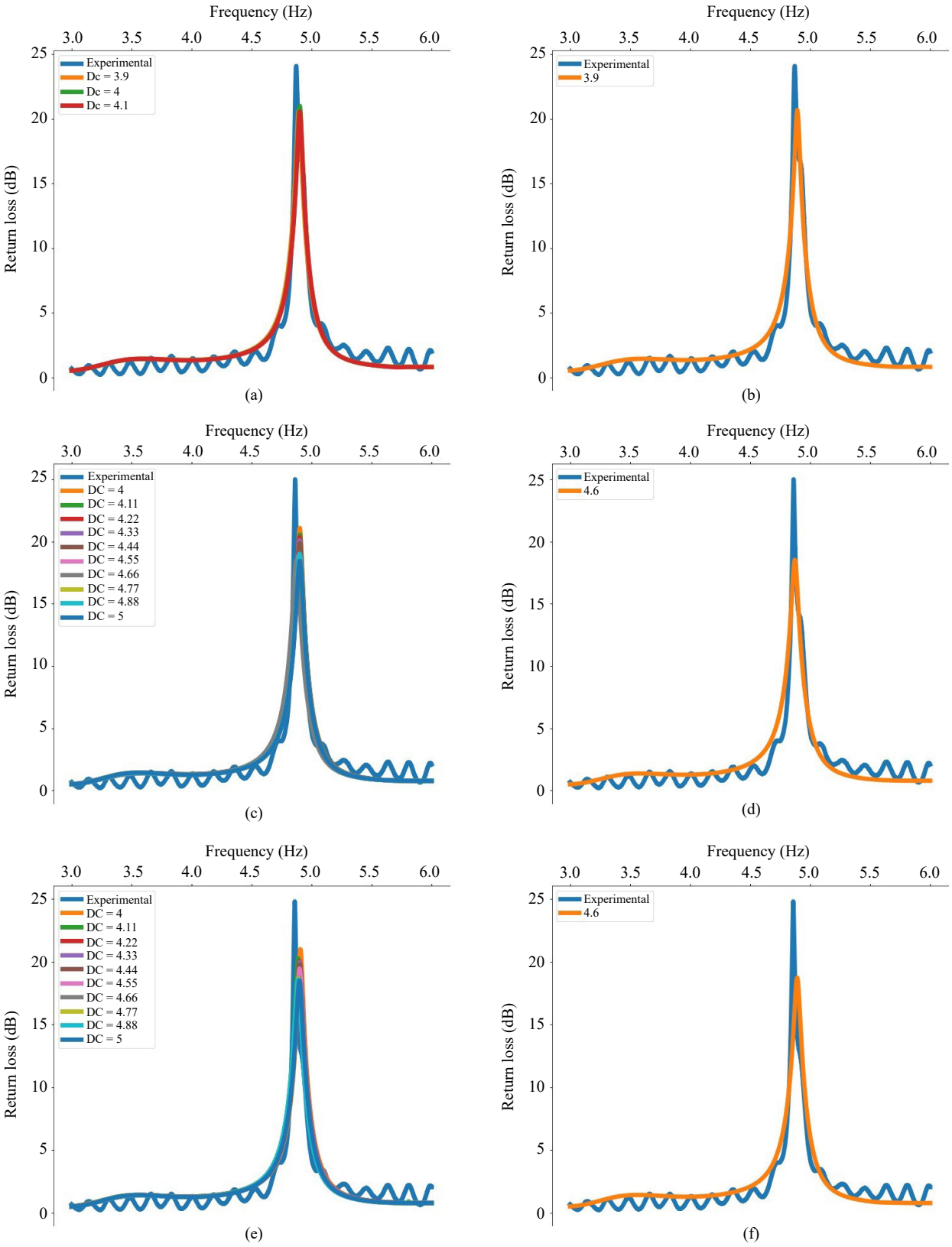

Figure 11. Far-field numerical vs. experimental results: (a) epoxy; (b) epoxy best fit; (c) 0.5 wt%; (d) 0.5 wt% best fit; (e) 1 wt%; (f) 1 wt% best fit

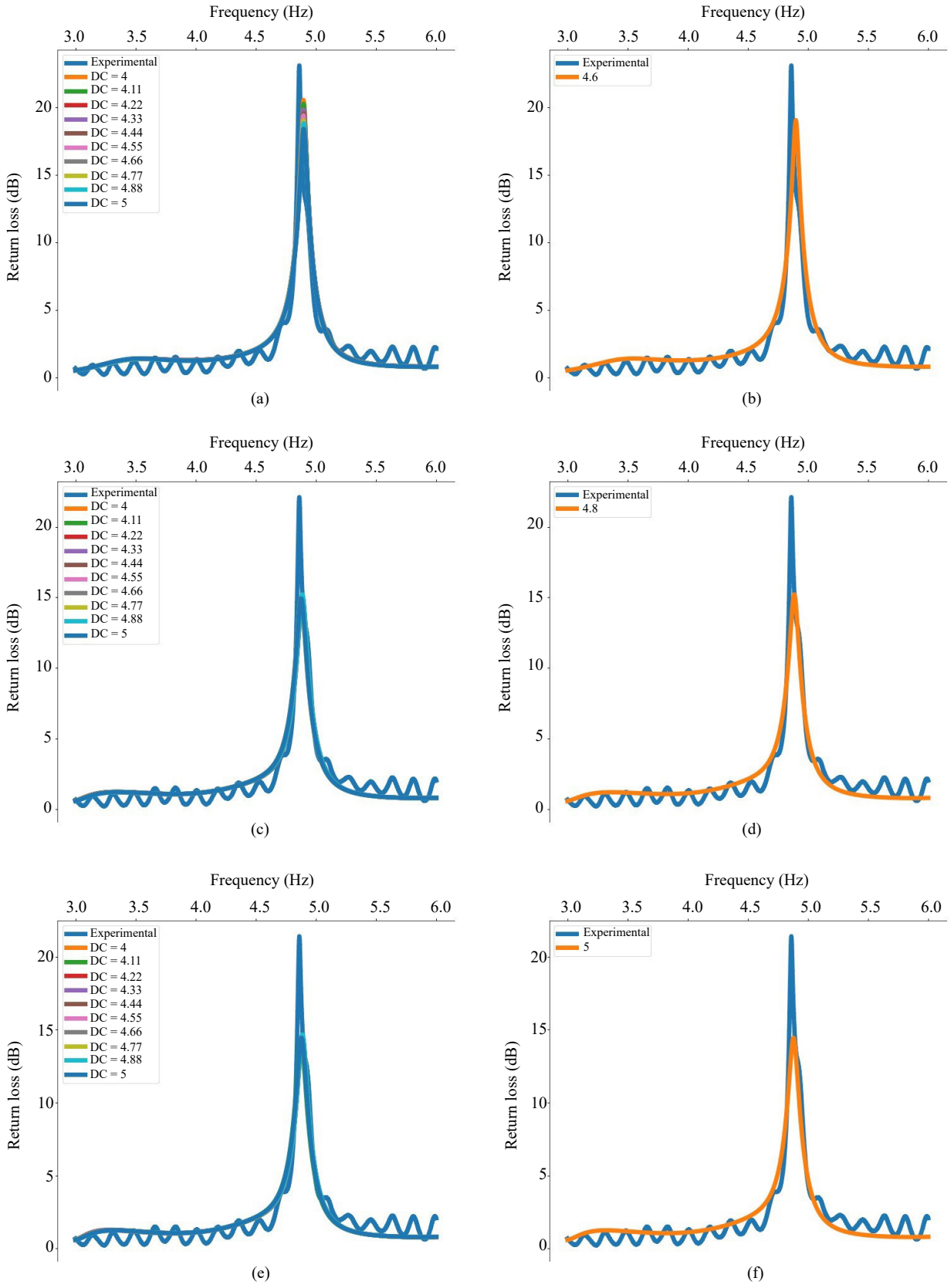

Figure 12. Far-field numerical vs. experimental results: (a) 2 wt%; (b) 2 wt% best fit; (c) 4 wt%; (d) 4 wt% best fit; (e) 5 wt%; (f) 5 wt% best fit

Conflict of interest

The author declares no conflict of interest.

References

[1] Iijima S. Helical microtubules of graphitic carbon. *Nature*. 1991; 354: 56-58. Available from: https://doi.org/10.1038/354056a0.

[2] Moniruzzaman M, Winey KI. Polymer nanocomposites containing carbon nanotubes. *Macromolecules*. 2006; 39(16): 5194-5205. Available from: https://doi.org/10.1021/ma060733p.

[3] Ek-Weis J, Eriksson A, Idda T, Olofsson N, Campbell EE. Radio-frequency characterization of varactors based on carbon nanotube arrays. *Proceedings of the Institution of Mechanical Engineers, Part N: Journal of Nanoengineering and Nanosystems*. 2008; 222(3): 111-115. Available from: https://doi.org/10.1243/17403499JNN122.

[4] Katsounaros A, Zhang J, Hao Y. Microwave modeling of single multi-wall carbon nanotubes. In: *2012 6th European Conference on Antennas and Propagation (EUCAP)*. Prague, Czech Republic: IEEE; 2012. p.2673-2676. Available from: https://doi.org/10.1109/EuCAP.2012.6206585.

[5] Katsounaros A, Rajab KZ, Hao Y, Mann M, Milne WI. X-band characterization of multi-walled carbon nanotube films. In: 2011 *International Conference on Electromagnetics in Advanced Applications*. Turin, Italy: IEEE; 2011. p.516-519. Available from: https://doi.org/10.1109/ICEAA.2011.6046394.

[6] Tarfaoui M, Lafdi K, El Moumen A. Mechanical properties of carbon nanotubes based polymer composites. *Composites Part B: Engineering*. 2016; 103: 113-121. Available from: https://doi.org/10.1016/j.compositesb.2016.08.016.

[7] El Moumen A, Tarfaoui M, Nachtane M, Lafdi K. Carbon nanotubes as a player to improve mechanical shock wave absorption. *Composites Part B: Engineering*. 2019; 164: 67-71. Available from: https://doi.org/10.1016/j.compositesb.2018.11.072.

[8] Tarfaoui M, Lafdi K, Beloufa I, Daloia D, Muhsan A. Effect of graphene nano-additives on the local mechanical behavior of derived polymer nanocomposites. *Polymers*. 2018; 10(6): 667. Available from: https://doi.org/10.3390/polym10060667.

[9] Liu C, Sergeichev I, Akhatov I, Lafdi K. CNT and polyaniline based sensors for the detection of acid penetration in polymer composite. *Composites Science and Technology*. 2018; 159: 111-118. Available from: https://doi.org/10.1016/j.compscitech.2018.02.028.

[10] Tamayo-Vegas S, Lafdi K. Experimental and modelling of temperature-dependent mechanical properties of CNT/polymer nanocomposites. *Materials Today: Proceedings*. 2022; 57(2): 607-614. Available from: https://doi.org/10.1016/j.matpr.2022.01.480.

[11] Tamayo-Vegas S, Muhsan A, Tarfaoui M, Lafdi K, Chang L. Effect of CNT additives on the electrical properties of derived nanocomposites (experimentally and numerical investigation). *Materials Today: Proceedings*. 2022; 52(2): 199-205. Available from: https://doi.org/10.1016/j.matpr.2021.09.361.

[12] Fang Q, Lafdi K. Effect of nanofiller morphology on the electrical conductivity of polymer nanocomposites. *Nano Express*. 2021; 2(1): 010019. Available from: https://doi.org/10.1088/2632-959X/abe13f.

[13] El Moumen A, Tarfaoui M, Lafdi K. Mechanical characterization of carbon nanotubes based polymer composites using indentation tests. *Composites Part B: Engineering.* 2017; 114: 1-7. Available from: https://doi.org/10.1016/j.compositesb.2017.02.005.

[14] Tarfaoui M, El Moumen A, Lafdi K, Hassoon OH, Nachtane M. Inter laminar failure behavior in laminate carbon nanotubes-based polymer composites. *Journal of Composite Materials*. 2018; 52(26): 3655-3667. Available from: https://doi.org/10.1177/0021998318767493.

[15] El Moumen A, Tarfaoui M, Lafdi K, Benyahia H. Dynamic properties of carbon nanotubes reinforced carbon fibers/epoxy textile composites under low velocity impact. *Composites Part B: Engineering*. 2017; 125: 1-8. Available from: https://doi.org/10.1016/j.compositesb.2017.05.

[16] El Moumen A, Tarfaoui M, Lafdi K. Computational homogenization of mechanical properties for laminate composites reinforced with thin film made of carbon nanotubes. *Applied Composite Materials*. 2018; 25: 569-588. Available from: https://doi.org/10.1007/s10443-017-9636-2.

[17] Ghodgaonkar DK, Varadan VV, Varadan VK. A free-space method for measurement of dielectric constants and loss

tangents at microwave frequencies. *IEEE Transactions on Instrumentation and Measurement*. 1989; 38(3): 789-793. Available from: https://doi.org/10.1109/19.32194.
[18] Qureshi Y, Tarfaoui M, Lafdi KK, Lafdi K. Nanotechnology and development of strain sensor for damage detection. In: Hassan MHM. (ed.) *Advances in Structural Health Monitoring*. IntechOpen; 2019. Available from: https://doi.org/10.5772/intechopen.82871.
[19] Liu C, Lafdi K. Environmental monitoring of composite durability use multiple sensing technologies. In: *CAMX – The Composites and Advanced Materials Expo Conference Proceedings*. Dallas: CAMX; 2018. p.1-13.
[20] Sebastian MT. *Dielectric materials for wireless communication*. United Kingdom: Elsevier; 2008.
[21] Tamayo-Vegas S, Lafdi K, Elsdon M. A contactless characterization of CNT/Epoxy nanocomposites behavior under acid exposure. *Composite Structures*. 2023; 305: 116508. Available from: https://doi.org/10.1016/j.compstruct.2022.116508.
[22] Yang L, Martin L, Staiculescu D, Wong CP, Tentzeris MM. Design and development of compact conformal RFID antennas utilizing novel flexible magnetic composite materials for wearable RF and biomedical applications. In: *2008 IEEE Antennas and Propagation Society International Symposium*. San Diego, CA, USA: IEEE; 2008. p.1-4. Available from: https://doi.org/10.1109/APS.2008.4619348.
[23] Duroc Y, Tedjini S. RFID: A key technology for Humanity. *Comptes Rendus Physique*. 2018; 19(1-2): 64-71. Available from: https://doi.org/10.1016/j.crhy.2018.01.003.
[24] Finkenzeller K, Waddington R. *RFID handbook*. England: Wiley; 2003.
[25] Tamayo-Vegas S, Muhsan A, Liu C, Tarfaoui M, Lafdi K. The effect of agglomeration on the electrical and mechanical properties of polymer matrix nanocomposites reinforced with carbon nanotubes. *Polymers*. 2022; 14(9): 1842. Available from: https://doi.org/10.3390/polym14091842.
[26] Thomas S, Thomas R, Zachariah AK, Mishra RK. (eds.) S*pectroscopic methods for nanomaterials characterization.* Netherlands: Elsevier; 2017.
[27] Afsar MN, Birch JR, Clarke RN, Chantry GW. The measurement of the properties of materials. *Proceedings of the IEEE*. 1986; 74(1): 183-199. Available from: https://doi.org/10.1109/PROC.1986.13432.
[28] Yaw KC. *Measurement of dielectric material properties—Application note*. Rohde & Schwarz; 2012 .
[29] Agilent Technologies. *Agilent 2-Port PNA-L Microwave Network Analyzer N5230A*. USA: Agilent Technologies; 2009.
[30] National Instruments RF Academy. *Introduction to Network Analyzer Measurements*. National Instruments; 2012.
[31] Balanis CA. *Antenna theory: Analysis and design*. 4th ed. USA: John Wiley & Sons; 2016.
[32] Páez EJ, Regina JP, Sandoval MD, Del Pino P, Tremola C, Azpúrua Auyanet MA. Theoretical and practical validation tests for a near-field to far-field transformation algorithm using spherical wave expansion. *Revista técnica de la Facultad de Ingeniería de la Universidad de Zulia*. 2012; 35(1): 109-118. Available from: http://hdl.handle.net/2117/28161.
[33] Lo YT, Lee SW. (eds.) *Antenna Handbook: theory, applications, and design*. New York: Springer; 2013. Available from: https://doi.org/10.1007/978-1-4615-6459-1.
[34] Capps C. Near field or far field? *EDN*. August 16 2001: p.95-99.
[35] Larsen FH. Probe correction of spherical near-field measurements. *Electronics Letters*. 1977; 14(13): 393-395. Available from: https://doi.org/10.1049/el:19770287.
[36] Computer Simulation Technology AG (CST). *CST Microwave Studio Workflow & Solver Overview*. CST; 2016.